Polymer 51 (2010) 5456–5461

Contents lists available at ScienceDirect

Polymer

journal homepage: www.elsevier.com/locate/polymer

Scanning electrochemical microscopy measurements of photopolymerized poly(ethylene glycol) hydrogels☆

Kavita M. Jeerage [a,*], Stephanie M. LaNasa [b], Holly A. Hughes [b], Damian S. Lauria [a], Stephanie J. Bryant [b], Andrew J. Slifka [a]

[a] Materials Reliability Division, National Institute of Standards and Technology, 325 Broadway, Boulder, CO 80305, USA
[b] Department of Chemical and Biological Engineering, University of Colorado, 424 UCB, Boulder, CO 80309, USA

ARTICLE INFO

Article history:
Received 4 June 2010
Received in revised form
4 September 2010
Accepted 12 September 2010
Available online 18 September 2010

Keywords:
Diffusivity
Hydrogel
Scanning electrochemical microscopy

ABSTRACT

Scanning electrochemical microscopy has been used to examine the molecular transport properties of photopolymerized poly(ethylene glycol) (PEG) hydrogels having different mesh sizes. Both the molecular weight (508 Da or 3000 Da) of the PEG diacrylate macromer and its weight percent (20 wt%, 40 wt%, or 60 wt%) in solution prior to photopolymerization were varied. Mesh size was estimated from equilibrium swelling measurements and a thermodynamic model. Estimated mesh sizes ranged from *ca.* 10 Å for 60 wt% PEG 508 gels to *ca.* 100 Å for 20 wt% PEG 3000 gels. The electrochemically active diffusing species, ferrocenemethanol, was detected via oxidation at a platinum microelectrode. For a given hydrogel, multiple approach curves showed a consistent relationship between current and distance. Electrochemically estimated diffusivities followed the same trend as predictions based on mesh size and ranged from 25% to 80% of the diffusivity in aqueous solution. As a proof of concept, scanning electrochemical microscopy was successfully used to map the topography of hydrogels with complex architecture, which are being designed as cell scaffolds.

Published by Elsevier Ltd.

1. Introduction

Hydrogels based on crosslinked poly(ethylene glycol) are important biomaterials being investigated for applications in drug delivery [1] and as cell scaffolds for tissue engineering [2]. This polymer offers many advantages including its biocompatibility and its ability to degrade if appropriate chemical groups are incorporated [1]. Poly(ethylene glycol) (PEG) hydrogels are typically formed from macromolecular divinyl monomers (*i.e.*, macromers) and crosslinked in the presence of an initiating system, such as a chemical photoinitiator and light. These hydrogels are versatile cell scaffold materials and can be used to encapsulate cells during the polymerization process [3,4] or can be fabricated with highly porous structures where cells are seeded onto the scaffold post-polymerization [5,6]. The mechanical and chemical environment experienced by cells will depend, in part, on the properties of the scaffold. In particular, the elasticity and swelling of hydrogels changes dramatically with the degree of crosslinking.

Diffusion of small molecules through the hydrogel network is critical to its function in many biological applications. For example, the oxygen permeability of contact lens materials is critical to supplying sufficient oxygen to the cornea, a nonvascular tissue [7]. New contact lens materials continue to be researched for extended wear [8] and new methods devised to measure oxygen permeability [9]. Another notable example is engineered cardiac muscle tissue, which demands high levels of oxygen due to the high metabolic activity of cardiomyocytes [10,11]. In general in tissue engineering, the structure of the scaffold plays a key role in the diffusion of nutrients, such as oxygen and glucose as well as larger species such as growth factors, which are important to cell survival, cell function, and tissue growth.

In crosslinked systems, the average distance between two neighboring crosslinks is termed the mesh size and dictates diffusion of molecules through hydrogels. Mesh size and other macroscopic properties are readily tuned by varying parameters such as the molecular weight of the divinyl macromer and the weight percent of macromer in solution prior to polymerization [12]. Mesh size is often estimated indirectly from equilibrium swelling measurements using the Flory–Rehner equilibrium-swelling theory [13]. However, this approach depends on a bulk measurement and does not provide information on spatial variations in the hydrogel structure. A variety of experimental techniques have been applied to

☆ Contribution of the U.S. Department of Commerce; not subject to copyright in the U.S.

* Corresponding author. Tel.: +1 303 497 4968; fax: +1 303 497 5030.
E-mail address: jeerage@boulder.nist.gov (K.M. Jeerage).

0032-3861/$ – see front matter Published by Elsevier Ltd.
doi:10.1016/j.polymer.2010.09.028

the characterization of diffusion in hydrogels, including confocal laser scanning microscopy [14] and nuclear magnetic resonance spectroscopy [15]. Electrochemical measurements possess the unique advantage of directly quantifying oxygen via its irreversible reduction on a platinum microelectrode surface. This is in contrast to optical methods and has been exploited for bulk measures of oxygen transmissibility and permeability [16].

Fan used microelectrodes to measure the diffusivities of several ferrocene derivatives within low wt% poly(acrylate) and poly (acrylamide) hydrogels [17]. In these studies, the electrode was pushed into the bulk gel to measure transient chronoamperometric curves. Hyk et al. measured diffusivities within 4 wt% poly(*N*-isopropylacrylamide) hydrogels, again pushing the electrode into the bulk gel [18]. However, the higher wt% poly(ethylene glycol) hydrogels studied here do not easily permit microelectrode insertion into the bulk gel. We instead utilize scanning electrochemical microscopy (SECM) [19] approach curves to investigate diffusive properties and to map changes in hydrogel architecture. It is well known that a microelectrode approaching a non-conductive, impermeable surface exhibits a decreased current due to blocking of the probe molecule by the surface. This is known as negative feedback and simulated approach curves have been produced by solving the steady-state diffusion equation for a variety of electrode geometries [20]. When the electrode approaches a permeable surface such as a hydrogel, the concentration profile is more complicated, with diffusion occurring through the solution and through the gel [21]. Several crosslinking densities were examined by varying the macromer molecular weight (508 Da or 3000 Da) as well as the macromer concentration (20 wt%, 40 wt%, or 60 wt%) in solution prior to polymerization. A small, neutral species, ferrocenemethanol ($FcCH_2OH$), is used as the electroactive probe molecule. Multiple locations are sampled to assess the homogeneity of the hydrogel structure, and electrochemically estimated diffusivities are compared with predictions from a thermodynamic model based on bulk equilibrium swelling measurements.

SECM has been applied in multiple ways to the imaging of living cells [20,22]. Depending on the redox mediator chosen, cell topography [23], intracellular redox activity [24,25], and oxygen profiles [26,27] can be mapped. $FcCH_2OH$ has recently been proposed as a superior redox mediator for metabolic activity [22,28,29]. These studies used cells cultured on polystyrene dishes, where the interaction between microelectrode and substrate is well understood. In tissue engineering, cells may be seeded onto porous scaffolds with complex architecture. Therefore the studies of PEG hydrogels presented here are critical to SECM investigations of cells in this more natural environment.

2. Experimental

2.1. PEG hydrogel preparation

PEGDA (poly(ethylene glycol) diacrylate) 508 was obtained commercially, whereas PEGDA 3000 was synthesized by the following procedure. PEG 3000 was added to a methylene chloride solution containing triethylamine on ice such that the molar ratio of triethylamine to PEG was 3:1. Acryloyl chloride diluted 10:1 in methylene chloride was added dropwise to this solution until the molar ratio of acryloyl chloride to PEG was 2.5:1. After addition of acryloyl chloride, the reaction proceeded overnight at room temperature. Product was separated and purified through precipitation in cold ethyl ether, desiccated for 48 h, and stored at 4 °C under argon. Chemical structure was confirmed by proton nuclear magnetic resonance spectroscopy.

For PEG 508 hydrogels, the macromer solution was made from PEGDA 508 and 41% ethylene glycol/59% water (v/v). For PEG 3000 hydrogels, the macromer solution was made from PEGDA 3000 and water. The photoinitiator 2,2-dimethoxy-2-phenyl-acetophenone was dissolved in 1-vinyl-2-pyrrolidinone to a final concentration of 500 mg/mL. This solution was added to the macromer solution such that the final photoinitiator concentration of the macromer solution was 1.5% (w/w). The final macromer + photoinitiator solution was added to a mold formed from glass slides and spacers, which constrain the polymerized gel to 0.76 mm (0.03 in) thickness. The solution was polymerized for 8 min under ultraviolet light (8 mW/cm^2) with a wavelength of 365 nm. Hydrogels of the following weight percents were studied: 20 wt%, 40 wt%, and 60 wt% (6 different formulations in total). The finished polymer was soaked in water for 24 h with several solution replacements. Fully hydrated scaffolds were punched into 10 mm diameter discs and stored in water until use.

Excess water was removed from 10 mm diameter hydrogels, then each was soaked in 10 mL of electrolyte containing the electroactive probe (0.001 mol/L $FcCH_2OH$ + 0.1 mol/L KCl) for at least 96 h prior to electrochemical measurements, with several solution replacements. Hydrogels were mounted in a polycarbonate cell using a thin layer of vacuum grease at its upper and lower edges. Both the upper and lower faces of the hydrogel contacted the electrolyte (0.001 mol/L $FcCH_2OH$ + 0.1 mol/L KCl) during scanning electrochemical microscopy (SECM details in 2.2). Distilled, deionized water was used for all macromer, electrolyte, and swelling solutions.

To create a porous hydrogel sample, uncrosslinked poly(methyl methacrylate) spheres were sieved to 150 μm to 180 μm in diameter and placed in a mold. After sonication for two 20 min intervals, the spheres were sintered for 19 h at 140 °C. The macromer solution used for 40 wt% PEG 508 hydrogels was added in stages to the entire volume of the mold and photopolymerized. After removing the polymer from the mold, the spheres were dissolved in a 1:1 acetone/methylene chloride solvent solution for approximately 48 h, with three solution changes. The finished polymer was then soaked in water for 24 h with several solution replacements and punched into 10 mm diameter discs. After examination of a hydrated sample via scanning electrochemical microscopy (SECM details in 2.2), the porous hydrogel was soaked in a 70% ethanol/water solution overnight and dried under vacuum (about 16.7 kPa) for 2 h at room temperature prior to examination via scanning electron microscopy (SEM) at 1.5 keV.

2.2. Scanning electrochemical microscopy (SECM)

Commercially available Pt disc microelectrodes surrounded by glass were polished with 50 nm alumina, rinsed with water, and dried in a stream of inert gas. The counter electrode was a Pt wire and the reference electrode was an Ag/AgCl wire in saturated KCl. All experiments utilized the reversible one electron oxidation of the neutral probe molecule ferrocenemethanol, which is diffusion limited at $E = 0.5$ V vs. Ag/AgCl. When the potential on the Pt microelectrode in a quiescent electrolyte is stepped to this potential, its current (I_{tip}) is described by an equation having time-dependent and time-independent terms. At steady state, the limiting current (I_{lim}) for a disc microelectrode surrounded by an insulator is described by the expression

$$I_{lim} = 4nFD_oCa \quad (1)$$

where n is the number of electrons transferred in the redox reaction [1], F is Faraday's constant [96484.6 C/mol], D_o is the diffusivity of ferrocenemethanol [6.8×10^{-6} cm^2/s], C is its bulk concentration [1×10^{-6} mol/cm^3], and a is the microelectrode radius [*ca.* 12.5×10^{-4} cm]. Prior to each series of measurements, the radius of

the microelectrode was determined by use of Eq. (1) and a redox species with known diffusivity.

Motion of the microelectrode in the x, y, and z directions was controlled by a closed-loop motorized stage using software written in house. Approach curves were acquired by moving the microelectrode towards the sample in 100 nm steps at 1.0 μm/s; the tip current was recorded after 50 ms of settling time. Prior to each series of measurements, the normalized current (I_{tip}/I_{lim}) vs. normalized distance (z/a) curve was measured as the microelectrode was brought into contact with a glass surface. This is known as pure negative feedback and the shape of the approach curve depends on the dimensions of the microelectrode and insulator, in particular, the ratio of the glass (insulator) radius to the microelectrode radius ($R_g = r_g/a$) [30]. Experimental measurements using a glass substrate were compared with simulated approach curves to verify that the plane of the probe tip was aligned with the plane of the substrate.

Since the exact location of the electrolyte/hydrogel interface was not known a *priori*, approach curves began at least 250 μm above the interface and continued for several micrometers into the bulk hydrogel before the microelectrode was retracted. The derivative of the current was used to identify the z position corresponding to an inflection point. This is the electrolyte/hydrogel interface and its position (normalized distance, z/a) was set to zero.

2.3. Equilibrium swelling measurements

The equilibrium mass swelling ratio ($q = m_s/m_d$) was determined by weighing swelled hydrogels (m_s), drying them under vacuum, then weighing the dried polymer (m_d). For each hydrogel formulation, equilibrium swelling measurements were performed on five samples. The volumetric swelling ratio (Q) was determined using known densities of polymer (ρ_p) and water (ρ_w) and

$$Q = 1 + (q-1)\frac{\rho_p}{\rho_w}. \tag{2}$$

We estimated the average molecular weight between crosslinks ($\overline{M}_c$) using a modified version of the Flory–Rehner Equation neglecting chain ends [13],

$$\frac{1}{\overline{M}_c} = -\frac{(\overline{\nu}/V_1[\ln(1-\nu_2)+\nu_2+\chi_{12}\nu_2^2])}{\left[\nu_2^{1/3}-\frac{\nu_2}{2}\right]}, \tag{3}$$

where $\overline{\nu}$ is the specific volume of the polymer [$\overline{\nu} = 1/\rho_p$], V_1 is the molar volume of water [l/mol], ν_2 is the equilibrium polymer volume fraction [$\nu_2 = 1/Q$], and χ_{12} is a polymer–solvent interaction parameter for poly(ethylene glycol) in water [0.426] [31]. Mesh size refers to the distance between two adjacent crosslinks and controls the maximum solute size that can diffuse thorough the gel. Mesh size (ξ) was estimated with

$$\xi = \nu_2^{-1/3} C_n^{1/2} \ln^{1/2}, \tag{4}$$

where C_n is the characteristic ratio of the polymer [2], l is the bond length [1.47], and n is the number of bonds between the crosslinks [$n = 3\overline{M}_c/\overline{M}_r$, where $\overline{M}_r$ is the molecular weight of the repeating unit]. Finally diffusivity in the hydrogel (D_g) is estimated from

$$D_g = \left(1-\frac{r_s}{\xi}\right)\exp\left(-\frac{\nu_2}{1-\nu_2}\right)D_o, \tag{5}$$

where r_s is the hydrodynamic radius of the solute. (For a more detailed discussion of Eq. (3)–(5), including their theory and the assumptions involved, the reader is referred to [32,33] and references therein.) The hydrodynamic radius can be estimated from the Stokes–Einstein Equation:

$$r_s = \frac{k_B T}{4\pi\eta D_o}. \tag{6}$$

In this equation k_B is the Boltzmann constant [1.38×10^{-23} J/K], T is the temperature [295 K], η is the solution viscosity [8.9×10^{-4} Pa s], and 4 replaces 6 in the denominator, as the solute molecules are not significantly larger than the solvent [34].

3. Results and discussion

Fig. 1 shows a representative set of cyclic voltammograms obtained far from the surface, pressed into the surface of a 60 wt% PEG 508 hydrogel, and again far from the surface upon retraction. Because these materials are highly elastic and because the insulated microelectrode isn't sharp, attempting to penetrate the microelectrode into the hydrogel was not successful. Instead, the gel deforms under the electrode. Far from the surface, the voltammogram reaches a steady-state, diffusion-limited current as expected; pressed into the hydrogel, the limiting current is much lower. Upon retraction, the original voltammogram is recovered. Fig. 1 shows that the microelectrode surface is not affected by contact with the hydrogel and can be used to sample multiple locations on a hydrogel without renewing the surface. By use of Eq. (1), D_o is $6.8 \pm 0.1 \times 10^{-6}$ cm^2/s. Approach curves were next measured as the microelectrode moved from the bulk electrolyte to the electrolyte/hydrogel interface.

3.1. SECM approach curves

Fig. 2 shows approach curves to 20 wt%, 40 wt%, and 60 wt% PEG 508 hydrogel surfaces. Far from the surface, the limiting current is stable (not shown in this figure; however currents were measured starting roughly 350 μm above the surface). Closer to the surface, the current decreases, but not nearly as much as predicted by simulations of pure negative feedback or by measurements under those conditions. At the surface, the current stabilizes again. As mentioned previously, since the hydrogel is elastic, the microelectrode deforms the gel rather than penetrating it, leading to the small current decrease seen in this figure. For these hydrogels, $FcCH_2OH$ is a reasonable probe molecule as both I_{tip}/I_{lim} during approach and at the surface are quite distinct. The 60 wt% gel is the

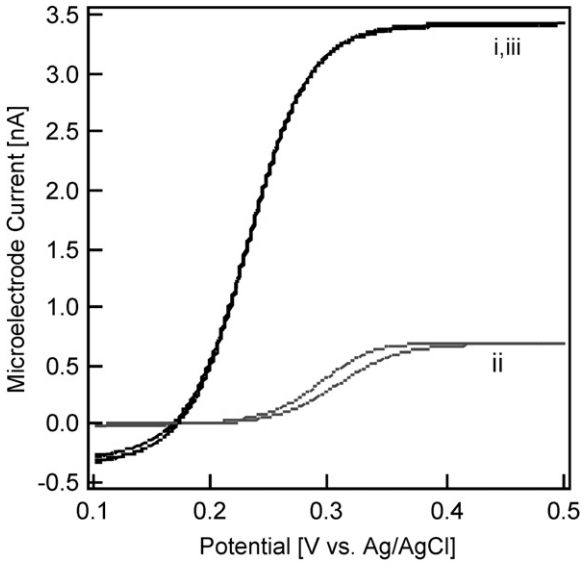

Fig. 1. Cyclic voltammograms were obtained at 2 mV/s in solution (i), in contact with the surface of a 60 wt% PEG 508 hydrogel (ii), and upon retraction (iii).

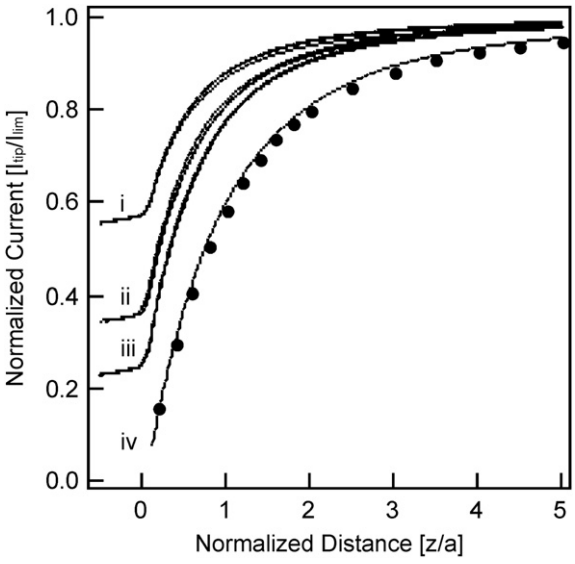

Fig. 2. Approach curves to 20 wt% (i), 40 wt% (ii), and 60 wt% (iii) PEG 508 hydrogel surfaces. For each hydrogel, three separate locations were sampled and plotted. In the fourth curve (iv) simulated currents for approach to an impermeable insulator are compared with experimental data for approach to a glass surface. Simulated data (filled circles) were calculated with the analytical approximation of Amphlett and Denault [30] for $R_g = 5.09$.

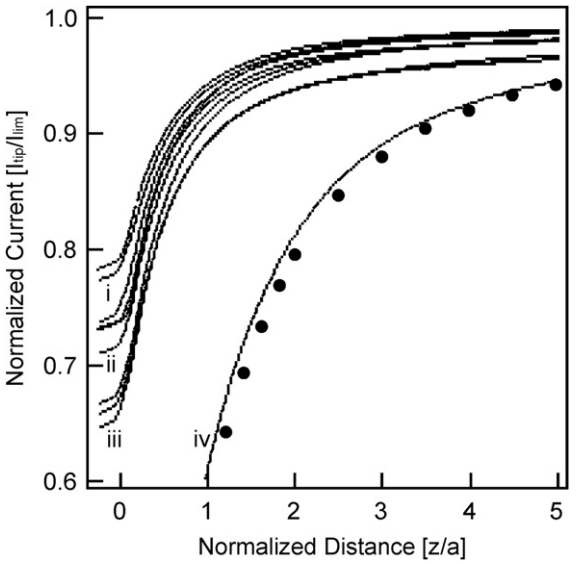

Fig. 3. Approach curves to 20 wt% (i), 40 wt% (ii), and 60 wt% (iii) PEG 3000 hydrogel surfaces. For each hydrogel, three separate locations were sampled and plotted. In the fourth curve (iv) simulated currents for approach to an impermeable insulator are compared with experimental data for approach to a glass surface. Simulated data (filled circles) were calculated with the analytical approximation of Amphlett and Denault [30] for $R_g = 5.09$.

strongest barrier (curve is closest to pure negative feedback), followed by the 40 wt% and 20 wt% gels.

To provide an indication of heterogeneity, three separate locations spaced 1 mm apart were sampled. All approaches are shown in Fig. 2 and there is almost no variation in the resulting curves. Several gels from different batches were also examined; they showed little variability and were omitted from Fig. 2 for clarity. Altogether, these results indicate a consistent relationship between current and distance for a given macromer weight percent, indicating little heterogeneity in the crosslinked structure. If there is within-gel spatial variation, it is on a smaller scale than that probed by this relatively large microelectrode.

Similar to other situations where feedback measurements have been used to image topography [35–38], the results in Fig. 2 indicate that the topography of permeable hydrogel substrates can be mapped electrochemically; however the current–distance relationship must first be determined for each formulation. Compared to pure negative feedback, I_{tip}/I_{lim} is greater for a given electrode–hydrogel distance. This limits the height of features that can be imaged by an electrode in one plane (constant height mode). For example, the distance from where the normalized current (I_{tip}/I_{lim}) reads 0.95 at a location above the PEG 508 hydrogel surface to its surface is 13.3 μm (20 wt%) to 15.9 μm (60 wt%) for an electrode of 5 μm radius, compared to 27 μm for pure negative feedback. This limitation can be countered by following the topography dynamically (constant current mode), which is necessary even in situations of pure negative feedback if the feature height is large [23].

Fig. 3 shows approach curves to 20 wt%, 40 wt%, and 60 wt% PEG 3000 hydrogel surfaces. Again simulated and experimentally measured currents for pure negative feedback are shown for comparison. For these hydrogels, $FcCH_2OH$ is less useful as a probe molecule. Although I_{tip}/I_{lim} at the surface is distinct, during approach the I_{tip}/I_{lim} curves are harder to distinguish, particularly for 20 wt% vs. 40 wt%. There is also greater variability within each hydrogel, reflecting irregularities in the mesh which occur with large macromers. For hydrogels with large average mesh sizes, macromer weight percent is expected to only have a minor effect on the diffusivity of a small species. This is reflected in the similarity of the approach curves. However, the trends in Fig. 3 match our expectations and there is still a fairly consistent current–distance relationship for mapping topography, though feature height would be limited to 6.7 μm (20 wt%) to 12.2 μm (60 wt%) for constant height imaging with an electrode of 5 μm radius.

3.2. $FcCH_2OH$ diffusion within hydrogel scaffolds

Table 1 shows swelling and crosslinking characteristics of the hydrogel mesh calculated from Eq. (2)–(4) and diffusivities estimated from Eq. (5). Five samples were averaged for each condition. Large mesh sizes imply solution-like diffusivity for small molecules. Even the smallest mesh size is nearly twice the estimated hydrodynamic radius of $FcCH_2OH$, leading to high predicted diffusivities that range from 16% to 82% of the diffusivity in aqueous solution. As the weight percent in the hydrogel decreases, its estimated mesh size (ξ) exhibits greater variability. This is particularly true of the 20 wt% gels, where ξ has about 10% uncertainty. However ξ has less impact on D_g when the ξ is large compared to the hydrodynamic radius (5.4 Å from Eq. (6)); therefore variability in the estimated diffusivities is 5% or less for all samples. Compared to typical hydrogels used for cell encapsulation, the gels studied here are highly crosslinked.

Determining diffusivities via Eq. (5) is very reliable if the hydrodynamic radius and mesh size are accurate. Despite its simplicity, the Stokes–Einstein Equation is often found to relate

Table 1
Volumetric swelling ratio (Q), average molecular weight between crosslinks ($\overline{M}_c$), mesh size (ξ), and diffusivity in the hydrogel (D_g).

Hydrogel	Q	$\overline{M}_c$ [Da]	ξ [Å]	D_g [cm^2/s]
20 wt% PEG 508	4.6 ± 0.3	1300 ± 200	47 ± 5	$4.6 \pm 0.2 \times 10^{-6}$
40 wt% PEG 508	2.60 ± 0.05	190 ± 20	17.9 ± 0.6	$2.7 \pm 0.1 \times 10^{-6}$
60 wt% PEG 508	1.92 ± 0.02	112 ± 4	10.1 ± 0.2	$1.08 \pm 0.05 \times 10^{-6}$
20 wt% PEG 3000	8.0 ± 0.6	4500 ± 800	100 ± 10	$5.6 \pm 0.1 \times 10^{-6}$
40 wt% PEG 3000	5.7 ± 0.3	2400 ± 300	69 ± 6	$5.1 \pm 0.1 \times 10^{-6}$
60 wt% PEG 3000	4.4 ± 0.1	1150 ± 70	43 ± 2	$4.44 \pm 0.07 \times 10^{-6}$

solution diffusivity and hydrodynamic radius surprisingly well [34]. However the model used to estimate mesh size from equilibrium swelling measurements was derived for hydrogels that exhibit point crosslinks. In these systems, the mesh size is directly related to the molecular weight between two neighboring crosslinks in the macromolecules. In hydrogels which are fabricated from large multifunctional macromers, the resulting network structures are much more complicated as point crosslinks are replaced by large poly(ethylene glycol) crosslinks. Limitations in classical theories have been discussed [39].

The steady-state approach curves measured in Figs. 2 and 3 are sensitive to both the concentration and diffusivity of $FcCH_2OH$ in the hydrogel. Situations in which concentration and diffusivity vary within two contacting phases have been treated theoretically [21]. In supporting experiments, chronoamperometric measurements within hydrogels were used to separate the relative contributions of concentration and diffusivity; Barker et al. found good correspondence between experimental and simulated approach curves generated using these values. In their experiments, the hydrogels were permselective for cationic probe molecules but excluded the anionic probe molecule. For a small, neutral species such as $FcCH_2OH$, it may be reasonable to assume that its concentration in the hydrogel is equivalent to its concentration in the contacting electrolyte. Then the ratio of the diffusivities (D_g/D_o) is equal to the ratio of the currents (I_{tip}/I_{lim}) at the interface, neglecting diffusion from above the plane of the microelectrode.

Fig. 4 compares diffusivities estimated in this manner with diffusivities predicted by equilibrium swelling; the values are strongly correlated. Fan's evaluation of diffusion in poly(acrylate) and poly(acrylamide) also assumed equivalent concentrations in the hydrogel and electrolyte [17], however, this analysis was limited to low wt% hydrogels (up to 20 wt%). Partitioning of $FcCH_2OH$ between the electrolyte and hydrogel phases may be affected here by the volume occupied by polymer in the hydrogel, which varies with macromer length and weight percent. Swelling measurements in Table 1 indicate that the volume occupied by polymer chains within swelled hydrogels ranges from 0.22 to 0.52 for PEG 508 hydrogels and 0.13 to 0.23 for PEG 3000 hydrogels. If the polymer volume fraction leads to a systematic decrease in $FcCH_2OH$ concentration within the hydrogel, estimating D_g from I_{tip}/I_{lim} should systematically under predict diffusivity. This is not seen in Fig. 4, suggesting that the assumption of equivalent concentrations is reasonable.

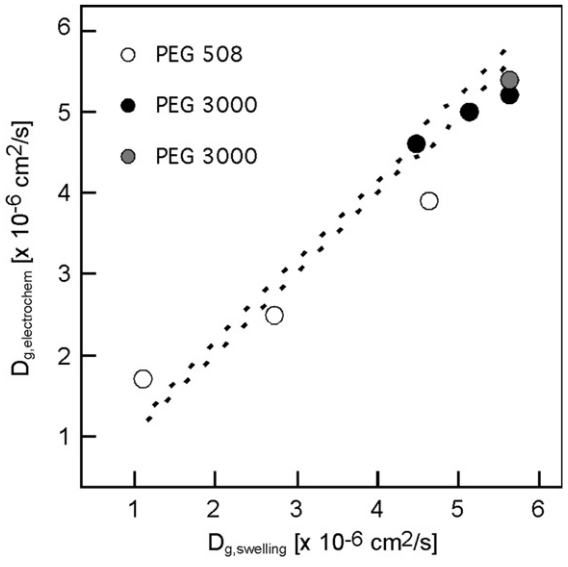

Fig. 4. Comparison of D_g estimated electrochemically vs. D_g predicted by equilibrium swelling. Pearson's linear correlation coefficient is 0.98. Dashed lines indicate the range of predicted values. Open circles are PEG 508 gels; filled circles are PEG 3000 gels. Gray circle is a 20 wt% PEG 3000 hydrogel from a different PEGDA synthesis.

3.3. Topography of porous hydrogel scaffolds

Porous PEG hydrogels are being developed as cell scaffolds through the use of various templating strategies [40,41]. We examined the top surface of several porous scaffolds, where the pores represent the fused regions of the sphere template, which is approximately 25% of the sphere diameter [42]. The large area image in Fig. 5a was obtained by scanning an electrode of 5 μm radius above the hydrogel surface. Above the porous surface, the current approaches the limiting current as the microelectrode is not sensitive to the lower boundaries of the pores, however the image clearly shows the regularity of the individual pore openings

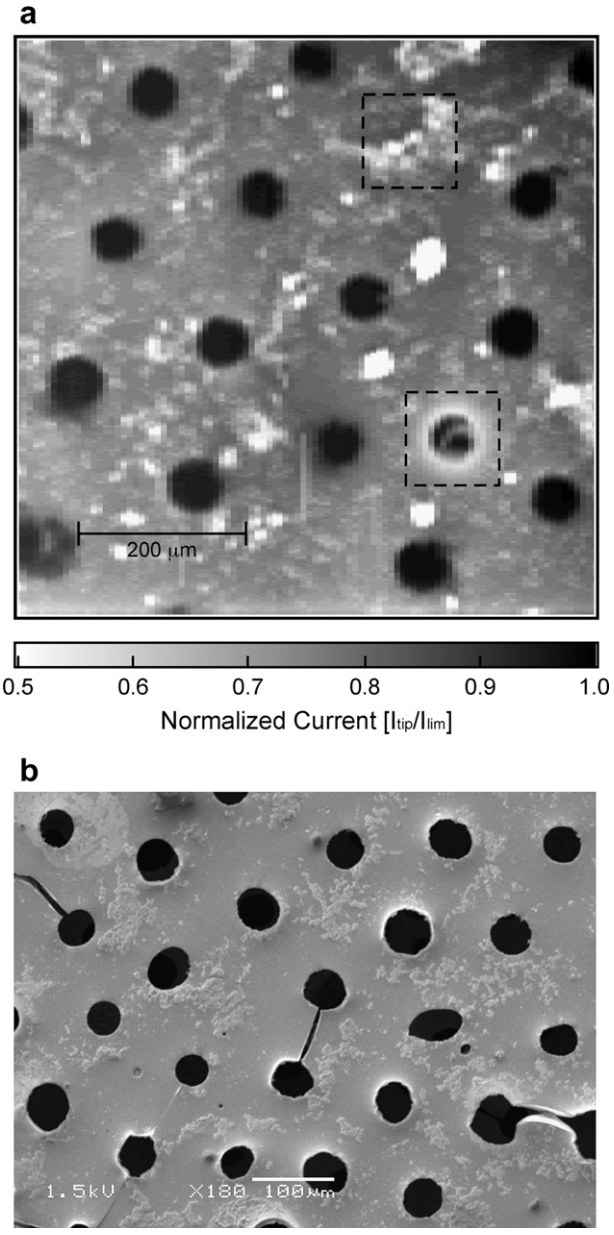

Fig. 5. SECM image of hydrated, 40 wt% PEG 508 hydrogel photopolymerized around a sphere template that has been dissolved (a) and SEM image of the same hydrogel (different region) after vacuum drying (b).

and their hexagonal spacing, indicative of a close-packed sphere template. The upper box highlights what appears to be a region where the bulk hydrogel formed over the pore; the lower box highlights a partially open pore. This and similar images provide confidence that we will be able to position microelectrodes for imaging cells on cross-sectioned porous scaffolds, work now in progress. Hydrogels with smaller pores (not shown) showed less regularity in pore spacing and produced more complicated images due to air trapped within some pore openings.

The scanning electron microscopy image in Fig. 5b was obtained after drying the hydrogel; cracks between pores are due to the vacuum drying process. It is possible to examine long-range order with such images and occasionally to see the bottom of a pore and the interconnect leading to the next pore. However the pore openings are distorted by drying and do not appear as uniformly round as they are when hydrated. Furthermore the uneven size and spacing of the pore openings do not match the uniform size and hexagonal organization seen in the hydrated image. SECM images, therefore, can provide information about hydrated polymer scaffolds that is complementary to SEM images.

4. Conclusions

Scanning electrochemical microscopy (SECM) has been used to examine the molecular transport properties of photopolymerized poly(ethylene glycol) (PEG) hydrogels having different mesh sizes. Both the molecular weight of the PEG diacrylate macromer and its weight percent in solution prior to photopolymerization were varied. Mesh size was estimated from equilibrium swelling measurements and used to predict the diffusivity of ferrocenemethanol, detectable via oxidation at a platinum microelectrode. SECM approach curves were used to identify the hydrogel surface and the normalized current used to estimate diffusivity within the hydrogel. These diffusivities followed the same trends as diffusivities predicted by equilibrium swelling measurements. Approach curves showed a consistent current–distance relationship that can be used to follow the topography of PEG hydrogel scaffolds.

Role of the funding source

The funding source had no role in the study design or in the collection, analysis, or interpretation of data. The manuscript was reviewed and approved by the NIST Editorial Review Board prior to submission.

Acknowledgements

Financial support for this work was provided by a University of Colorado – National Institute of Standards & Technology (CU-NIST) Seed Grant. This research was performed while K.M.J. held a National Research Council (NRC) Postdoctoral Fellowship and S.M.L. held a National Science Foundation (NSF) Graduate Research Fellowship.

References

[1] Sawhney AS, Pathak CP, Hubbell JA. Macromolecules 1993;26(4):581–7.
[2] Drury JL, Mooney DJ. Biomaterials 2003;24(24):4337–51.
[3] Elisseeff J, McIntosh W, Anseth K, Riley S, Ragan P, Langer RJ. Biomed Mater Res 2000;51(2):164–71.
[4] Mann BK, Gobin AS, Tsai AT, Schmedlen RH, West JL. Biomaterials 2001; 22(22):3045–51.
[5] Hoque ME, Hutmacher DW, Feng W, Li S, Huang MH, Vert M, et al. J Biomater Sci Polym Ed 2005;16(12):1595–610.
[6] Lee WK, Ichi T, Ooya T, Yamamoto T, Katoh M, Yui NJ. Biomed Mater Res Part A 2003;67A(4):1087–92.
[7] Holden BA, Mertz WG. IOVS 1984;25(10):1161–7.
[8] Yoo MK, Choi YJ, Lee JH, Wee WR, Cho CS. J Drug Deliv Sci Technol 2007; 17(1):81–5.
[9] Obendorf D, Wilhem M. Anal Chem 2003;75(6):1374–81.
[10] Carrier RL, Rupnick M, Langer R, Schoen FJ, Freed LE, Vunjak-Novakovic G. Biotechnol Bioeng 2002;78(6):617–25.
[11] Radisic M, Malda J, Epping E, Geng WL, Langer R, Vunjak-Novakovic G. Biotechnol Bioeng 2006;93(2):332–43.
[12] Bryant SJ, Anseth KS. J Biomed Mater Res 2001;59(1):63–72.
[13] Flory PJ. Principles of polymer chemistry. Ithaca, NY: Cornell University Press; 1953.
[14] Watkins AW, Anseth KS. Macromolecules 2005;38(4):1326–34.
[15] Salvati A, Soderman O, Lynch IJ. Phys Chem B 2007;111(25):7367–76.
[16] Compan V, Guzman J, Riande E. Biomaterials 1998;19(23):2139–45.
[17] Fan F-RF. J Phys Chem B 1998;102(49):9777–82.
[18] Hyk W, Karbarz M, Stojek Z, Ciszkowska MJ. Phys Chem B 2004;108(3):864–8.
[19] Bard AJ, Fan F-RF, Kwak J, Lev O. Anal Chem 1989;61:132–8.
[20] Sun P, Laforge FO, Mirkin MV. Phys Chem Chem Phys 2007;9(7):802–23.
[21] Barker AL, Macpherson JV, Slevin CJ, Unwin PR. J Phys Chem B 1998;102 (9):1586–98.
[22] Bard AJ, Li X, Zhan W. Biosens Bioelectron 2006;22(4):461–72.
[23] Liebetrau JM, Miller HM, Baur JE. Anal Chem 2003;75(3):563–71.
[24] Liu B, Cheng W, Rotenberg SA, Mirkin MV. J Electroanal Chem 2001;500 (1–2):590–7.
[25] Liu B, Rotenberg SA, Mirkin MV. PNAS 2000;97(18):9855–60.
[26] Torisawa Y, Kaya T, Takii Y, Oyamatsu D, Nishizawa M, Matsue T. Anal Chem 2003;75(9):2154–8.
[27] Kaya T, Torisawa Y, Oyamatsu D, Nishizawa M, Matsue T. Biosens Bioelectron 2003;18(11):1379–83.
[28] Zhao Z, Petersen NO, Ding Z. Can J Chem 2007;85(3):175–83.
[29] Li X, Bard AJ. J Electroanal Chem 2009;628(1–2):35–42.
[30] Amphlett JL, Denault GJ. Phys Chem B 1998;102(49):9946–51.
[31] Canal T, Peppas NA. J Biomed Mater Res 1989;23(10):1183–93.
[32] Peppas NA. Hydrogels in medicine and pharmacy. Boca Raton, FL: CRC Press; 1986.
[33] Peppas NA, Hilt JZ, Khademhosseini A, Langer R. Adv Mater 2006;18(11): 1345–60.
[34] Levine IN. Physical chemistry. 4th ed. New York, NY: McGraw-Hill Inc,; 1995.
[35] Zhang M, Girault HH. Analyst 2009;134(1):25–30.
[36] Yasukawa Y, Kaya T, Matsue T. Anal. Chem 1999;71:4637–41.
[37] Macpherson JV, Beeston MA, Unwin PR. Langmuir 1995;11:3959–63.
[38] Laforge FO, Velmurugan J, Wang YX, Mirkin MV. Anal Chem 2009;81(8): 3143–50.
[39] Weber LM, Lopez CG, Anseth KS. J Biomed Mater Res Part A 2009;90A:720–9.
[40] Marshall AJ, Ratner BD. AIChE J 2005;51(4):1221–32.
[41] Agrawal CM, Ray RB. J Biomed Mater Res 2001;55(2):141–50.
[42] Bryant SJ, Cuy JL, Hauch KD, Ratner BD. Biomaterials 2007;28(19):2978–86.